

## Evolution and Morphology of Two Splitting Thunderstorms with Dominant Left-Moving Members

RODGER A. BROWN

*NOAA, Environmental Research Laboratories, National Severe Storms Laboratory, Norman, Oklahoma*

REBECCA J. MEITÍN

*Cooperative Institute for Research in Environmental Sciences, Boulder, Colorado*

(Manuscript received 14 June 1993, in final form 28 January 1994)

### ABSTRACT

During the late afternoon and early evening of 27 June 1989, three splitting thunderstorms formed over Standing Rock Indian Reservation in the southern portion of the North Dakota Thunderstorm Project area. The first two storms are the subject of this study. The entire life cycles of both storms were documented using a single ground-based Doppler radar. Radar reflectivity signatures of updraft summits and Doppler velocity signatures of divergence near storm top were used to deduce updraft evolution within the storms. Dual-Doppler radar observations from a ground-based radar and an airborne Doppler radar provided fragmentary documentation of the storms' life cycles.

The splitting storms on that day were unusual in two distinct ways: (a) the left members of the splitting storms were the dominant and longer-lasting ones, and (b) none of the deduced updrafts were collocated with centers of vorticity signatures that would have indicated updraft rotation. Both of the left-moving storms had 10 sequential primary updrafts, whereas their right-hand counterparts had 3 or 4 primary updrafts. Initial formation of the right-flank updrafts lagged behind the initial formation of the left-flank updrafts by 40–70 min. All the individual updraft summits moved in the general direction of the mean wind. Sequential updraft development on the left and right flanks of the storms suggested that expanding gust fronts provided the propagational component of storm motion.

### 1. Introduction

In his radar study of thunderstorms in the vicinity of Montreal, Hirschfeld (1960) was among the first to note in the radar reflectivity pattern of an isolated thunderstorm that the storm can split into two storms moving along divergent tracks. Although many studies of storm splitting have been undertaken since then, only in a few of them have Doppler radar measurements been made within one or both members of the splitting storm pair. The Doppler radar data typically reveal a cyclonically rotating updraft in the dominant right-moving storm and an anticyclonically rotating updraft in the weaker left-moving storm. These and other characteristics of splitting storms are discussed in section 2.

This study documents the entire life cycles of two splitting thunderstorms based on ground-based single-Doppler radar coverage. Limited portions of the life

cycles were based on dual-Doppler radar coverage from the ground-based radar and an airborne Doppler radar. The storms formed over Standing Rock Indian Reservation along the border between North and South Dakota on 27 June 1989 during the North Dakota Thunderstorm Project (Boe et al. 1992). The various data sources and analysis techniques used in this study are discussed in section 3. The environment within which the storms formed is discussed in section 4.

The two splitting storms (as well as a third one that is the subject of another study) that occurred on 27 June 1989 were unusual for two reasons. Foremost, the left member of each split was the taller and longer-lasting member, in contrast to the typical situation where the right member is the dominant one. Second, none of the updrafts in the two storms studied here appeared to rotate (that is, updraft collocated with vertical vorticity) during their mature stage. However, a pair of counterrotating vortices (rotating about vertical axes) developed on the midaltitude lateral flanks of most updrafts.

The finescale temporal resolution (Doppler radar volume scans every 3–5 min) in this study permitted documentation of discrete propagation of updraft sum-

---

*Corresponding author address:* Dr. Rodger A. Brown, NOAA, National Severe Storms Laboratory, 1313 Halley Circle, Norman, OK 73069.

mits within the storms. Details concerning these storms and their dominant updrafts (deduced from radar reflectivity and Doppler velocity divergence signatures at updraft summits) are discussed in sections 5 and 6. Section 7 is a concluding discussion.

## 2. Characteristics of splitting thunderstorms

The largest documented outbreak of splitting storms occurred on 25 August 1965, when seven splits took place during the afternoon in east-central Iowa with several of the storms moving into Illinois (Achtemeier 1969). However, the most unusual documented splitting process occurred on 3 April 1964 in northwest Texas and southwest Oklahoma (e.g., Wilk 1966; Fujita and Grandoso 1968; Charba and Sasaki 1971). Not only did an isolated storm split but both the right mover and left mover split, and the left-mover's right mover split produced a third-generation pair of diverging storms. One of the second-generation right movers produced the devastating Wichita Falls tornado. This splitting storm event was modeled numerically by Wilhelmson and Klemp (1981).

Burgess et al. (1976) tabulated the basic characteristics of 16 splitting storm pairs documented in the literature; this tabulation has been updated to 31 pairs and is listed in the appendix. Table 1 summarizes some of the characteristics of these right-moving and left-moving storms. On average, storms that moved to the right of the mean wind (typically density- or pressure-weighted mean from cloud base to the tropopause) deviated  $29^\circ$  at a speed of  $11 \text{ m s}^{-1}$ . Left-moving storms deviated an average of  $26^\circ$  at  $17 \text{ m s}^{-1}$ . In fact, the left-moving member of every splitting storm pair in Table A1 moved faster than its right-moving counterpart. Both right movers and left movers produced hail, but only the right movers consistently produced tornadoes. Most storms probably produced damaging winds, but that fact most likely was overlooked by storm reporters because hail or tornado damage was more noteworthy.

Evolution of the radar reflectivity patterns during and following the splitting process is quite predictable. Achtemeier (1969) likened the process to mitosis and cytokinesis observed in biological cells. He proposed the following sequence of events for storms, as amplified by Burgess et al. (1976):

1) Formation stage. A thunderstorm develops and propagates generally eastward or northeastward, not necessarily in the direction of the mean wind. A pronounced radar reflectivity gradient appears along the storm's rear flank.

2) Elongation stage. The thunderstorm elongates to an elliptical shape and the major axis of the ellipse is generally perpendicular to the direction of storm motion. During this stage, splitting of the intense reflectivity core is observed. The "split cores" grow apart

TABLE 1. Statistics of post-split severe thunderstorms based on tabulations in the appendix. Standard deviations are in parentheses.

Parameters	Right mover	Left mover
Average deviation from mean wind	$29^\circ$ ( $20^\circ$ )	$26^\circ$ ( $15^\circ$ )
Average storm speed ( $\text{m s}^{-1}$ )	11 (4)	17 (5)
Average storm duration (h)	2–3	2
Severe weather: hail ( $\geq 1.9 \text{ cm}$ )	65%	50%
damaging wind	>17%	>7%
tornado	40%	10%
Number of storms	31	31

and the reflectivity gradients intensify along the left and right storm flanks.

3) Splitting stage. The central portion of the echo rapidly diminishes in size and intensity. This dissipation leaves two separate thunderstorm cells.

4) Deviation stage. To a viewer looking along the direction of motion, the left member moves noticeably to the left of the mean wind direction and increases in speed. Conversely, the right member moves noticeably to the right of the mean wind and decreases in speed. Owing to the deviate motion, a considerable horizontal distance develops between the two echoes.

The relatively few Doppler radar studies of splitting thunderstorms (e.g., Brown et al. 1973; Burgess et al. 1976; Bluestein and Sohl 1979; Burgess 1981; Conway and Weisman 1988; Kubesh et al. 1988; Bluestein and Woodall 1990; Brown 1992) indicate that it is typical for the updraft in the right-moving storm to be rotating cyclonically and the updraft in the left-moving storm to be rotating anticyclonically. However, in some of the cited cases, the vorticity collocated with the updraft was not strong enough to have it categorized as a mesocyclone. Nominal threshold vorticity values for mesocyclones are a function of radar resolution and vary from roughly  $1 \times 10^{-2} \text{ s}^{-1}$  near the radar to  $5 \times 10^{-3} \text{ s}^{-1}$  at distances of 200 km or more (e.g., Vasiloff et al. 1993).

## 3. Data sources and analysis techniques

The data used in this study were obtained during the North Dakota Thunderstorm Project that took place from 12 June through 22 July 1989 in south-central North Dakota. The locations of the data sensors relative to the Standing Rock storms are shown in Fig. 1. The Cross-chain Loran Atmospheric Sounding System (CLASS) rawinsonde data and the Portable Automated Mesonet (PAM) surface data from the National Center for Atmospheric Research (NCAR) were collected at Elgin and Goodrich. National Weather Service (NWS) surface and rawinsonde data were collected at Bismarck.

NCAR's CP-3 and CP-4 Doppler radars were located in Bismarck and near Center, North Dakota, respec-

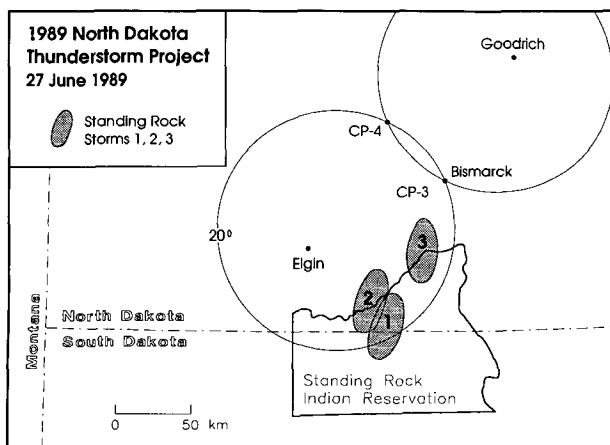


FIG. 1. The North Dakota Thunderstorm Project area during June and July 1989. The areas traversed by Standing Rock storms 1, 2, and 3 are indicated by shaded ovals. The region within the two circles, excluding the small overlap region between the radars, is the dual-Doppler coverage area where angles between the radar beams from CP-3 and CP-4 radars intersect at  $20^\circ$  or more and  $160^\circ$  or less. Rawinsonde and surface observational sites were located at Goodrich, Bismarck, and Elgin.

tively. Though all or most of each Standing Rock storm was within the nominal dual-Doppler coverage area (between-beam angles greater than or equal to  $20^\circ$ ), storms 1 and 2 were more than 120 km from CP-4, making the data too coarse for good dual-Doppler computations. (The lowest data were 2 km above the ground, and the radar beamwidth was greater than 2 km.) Dual-Doppler data for these two storms were obtained from the National Oceanic and Atmospheric Administration (NOAA) WP-3D airborne Doppler radar and the ground-based CP-3 Doppler radar. Table 2 gives the characteristics of both radars.

Since the airborne Doppler radar scans in a vertical plane normal to the aircraft's fuselage, ideal dual-Doppler geometry occurs when the aircraft flies in a radial direction directly toward or away from the ground-based radar. Between 1820 and 1926 CST 27 June, the WP-3D aircraft flew around and between the two splitting storms of interest (Fig. 2). On eight flight legs, the airborne radar was oriented  $40^\circ$ – $90^\circ$  from the radial viewing direction of the ground-based radar. Dual-Doppler analyses were performed at the following common reference times: 1822, 1833, 1837, 1844, 1854, 1905, 1920, and 1924 CST.

The velocity data from each radar were edited to remove noticeably bad values and to dealias velocity values. This was done using a combination of automatic dealiasing (Eilts and Smith 1990) and user-interactive dealiasing and error checks.

When radar data are interpolated to a common reference time, it is necessary to assume that the reflectiv-

TABLE 2. Characteristics of NOAA airborne WP-3D and NCAR ground-based CP-3 Doppler radars.

	WP-3D radar	CP-3 radar
<b>Transmitter</b>		
Frequency (MHz)	$9315 \pm 11.6$	5500
Wavelength (cm)	3.22	5.45
Pulse width ( $\mu$ s)	0.5	1.0
Pulse repetition frequency (Hz)	1600	750–1667
Peak power (kW)	60	400/1000
<b>Receiver</b>		
Dynamic range (dB)	80	100
<b>Antenna</b>		
Beamwidth—horizontal (deg)	1.35	1.02
Beamwidth—vertical (deg)	1.9	1.02
Gain, main beam (dB)	40	42.6
First sidelobe (dB)	–23	–23
Rotation rate ( $\text{deg s}^{-1}$ )	48	0–25 azimuth 0–15 elevation
First trip range (km)	76	90–200
Nyquist velocity ( $\text{m s}^{-1}$ )	13	10–23

ity and three-dimensional flow fields are not changing during the time it takes the radar to make a full three-dimensional scan of the storm. To help satisfy that assumption, data collection should be fast enough so that there is not appreciable evolution of the fields during the scanning time. The CP-3 radar typically scanned a

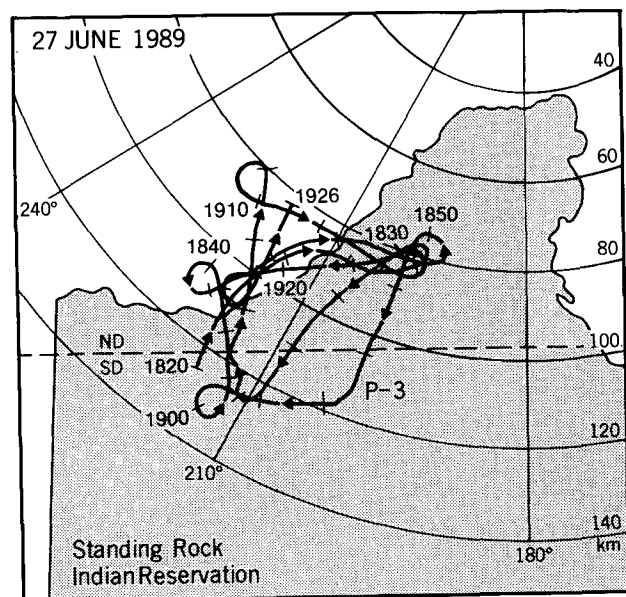


FIG. 2. Flight path of the WP-3D aircraft in the vicinity of Standing Rock storms 1 and 2. Times along the path are CST; tick marks are at 2-min intervals. The polar grid indicates range and azimuth from the CP-3 radar in Bismarck.

storm in 3 min, and the P-3 airborne radar took 3–6 min, so the fields should not have changed much during dual-Doppler data collection times.

The edited radar data then were interpolated to a three-dimensional grid array where dual-Doppler analyses were performed (Jorgensen et al. 1983). A motion vector of  $5 \text{ m s}^{-1}$  from  $270^\circ$  was used to spatially adjust the data to a common reference time. The resulting horizontal wind vectors were again edited interactively to remove any vectors that appeared to be erroneous; erroneous values often were found near the flight track.

Since the dual-Doppler analysis technique requires quasi-horizontal Doppler velocity measurements, only aircraft data within  $60^\circ$  above and below the flight altitude were used. Therefore, to sample an entire storm, the aircraft ideally should be at an altitude midway between the ground and storm top and at least as far away from the storm as storm top is above the aircraft. On this day, the aircraft was flying low (2.5 km above ground level) and often was closer than 10 km from one or both of the storms. As a result, the updrafts either were only partially sampled or were not sampled at all because they were completely outside the dual-Doppler coverage area. However, dual-Doppler data did permit the reconstruction of the flow fields downwind of the updrafts.

To compensate for the loss of information about the strength and location of updrafts, single-Doppler velocity and reflectivity signatures from the ground-based CP-3 radar were used to estimate updraft location and relative strength. This dataset (consisting of 43 volume scans) was independently processed and analyzed using the multiple-Doppler radar analysis (RADAN) system (e.g., Brown et al. 1981).

The primary Doppler velocity signature used in this study was that for divergence near the top of the updraft (e.g., Brown and Wood 1991). Occasionally, there was sufficient radar return at low altitudes to detect the signature of convergent flow into the lower portion of the updraft. The reflectivity signature used for an updraft was the top of a rising maximum in the horizontal reflectivity field produced by hydrometeors that formed in the upper portions of the updraft and that were carried upward by the vertically growing current.

#### 4. Environmental situation

The research area of the North Dakota Thunderstorm Project in south-central North Dakota was under the influence of a 500-mb ridge on 27 June 1989. At 1800 CST, the 500-mb high was centered over northern Mexico. The ridge extended sharply northward, and the ridge axis was lying just to the west of Bismarck.

On the morning of 27 June, a very weak warm front extended from a surface low in Alberta through west-central Montana and across central South Dakota. There was not much temperature contrast across the

front but the air south of the front was considerably more moist. The front moved northward during the day and by early afternoon was along the northern border of South Dakota. The satellite photos in Fig. 3 show the evolution (at 60–75-min intervals) of a north–south line of thunderstorms in South Dakota and northern Nebraska that formed in the moist air south of the front. The storms of interest in this study developed at the northern end of this line and are identified in Figs. 3c,d.

The dewpoint temperature and wind plots in Fig. 4 document the northward progression of the front and the moist air behind it from 1800 CST 26 June through 1800 CST 28 June. The stations in the plot are aligned from Elgin to the southwest through Bismarck to Goodrich to the northeast (refer to Fig. 1). The plots show an increase in dewpoint temperature during the morning of 27 June. Dewpoint temperatures of about  $15^\circ\text{C}$  at Elgin during the afternoon and evening of 27 June marked the northern extent of the moist air that led to the formation of thunderstorms (including Standing Rock storms 1, 2, and 3) that occurred in South Dakota and extended just across the border into North Dakota (Fig. 3). During the morning of 28 June, increasingly strong southeasterly winds brought the moist air farther north into central North Dakota, where severe thunderstorms occurred in the project area during the afternoon and evening of 28 June (Boe and Johnson 1990).

The atmospheric soundings closest in time and space to the Standing Rock storms were the CLASS rawinsonde released at Elgin at 1430 CST and the operational NWS rawinsonde released at Bismarck at 1800 CST 27 June, both of which were ahead of the warm front. The Elgin sounding (Fig. 5) reveals a lapse rate that is nearly dry adiabatic from the surface to 600 mb, which is favorable for convection. The relatively dry air shown at the surface in Fig. 4 extends upward through most of the sounding.

The Elgin soundings at 0830, 0923, and 1130 CST the next morning (not shown) indicate that temperatures below 600 mb and above the eroding nocturnal surface inversion had increased by  $2^\circ\text{--}3^\circ\text{C}$  following warm front passage. Moisture between the surface and 850 mb was steadily increasing, as also reflected by the surface measurements in Fig. 4. The layer from 850 to 700 mb was drier than indicated in Fig. 5. On the other hand, the layer from 700 to 300 mb was moister, probably reflecting residual moisture from the storms on 27 June.

A composite hodograph was prepared from the 1430 CST Elgin and 1800 CST Bismarck soundings by smoothing the average  $u$  and  $v$  components (Fig. 6). The density-weighted mean wind in the 1–12-km layer for the composite hodograph is  $268^\circ$  at  $6.5 \text{ m s}^{-1}$ . Overall, the hodograph is essentially a straight line, the type that numerical models indicate should produce a symmetric pair of splitting storms (e.g., Rotunno and

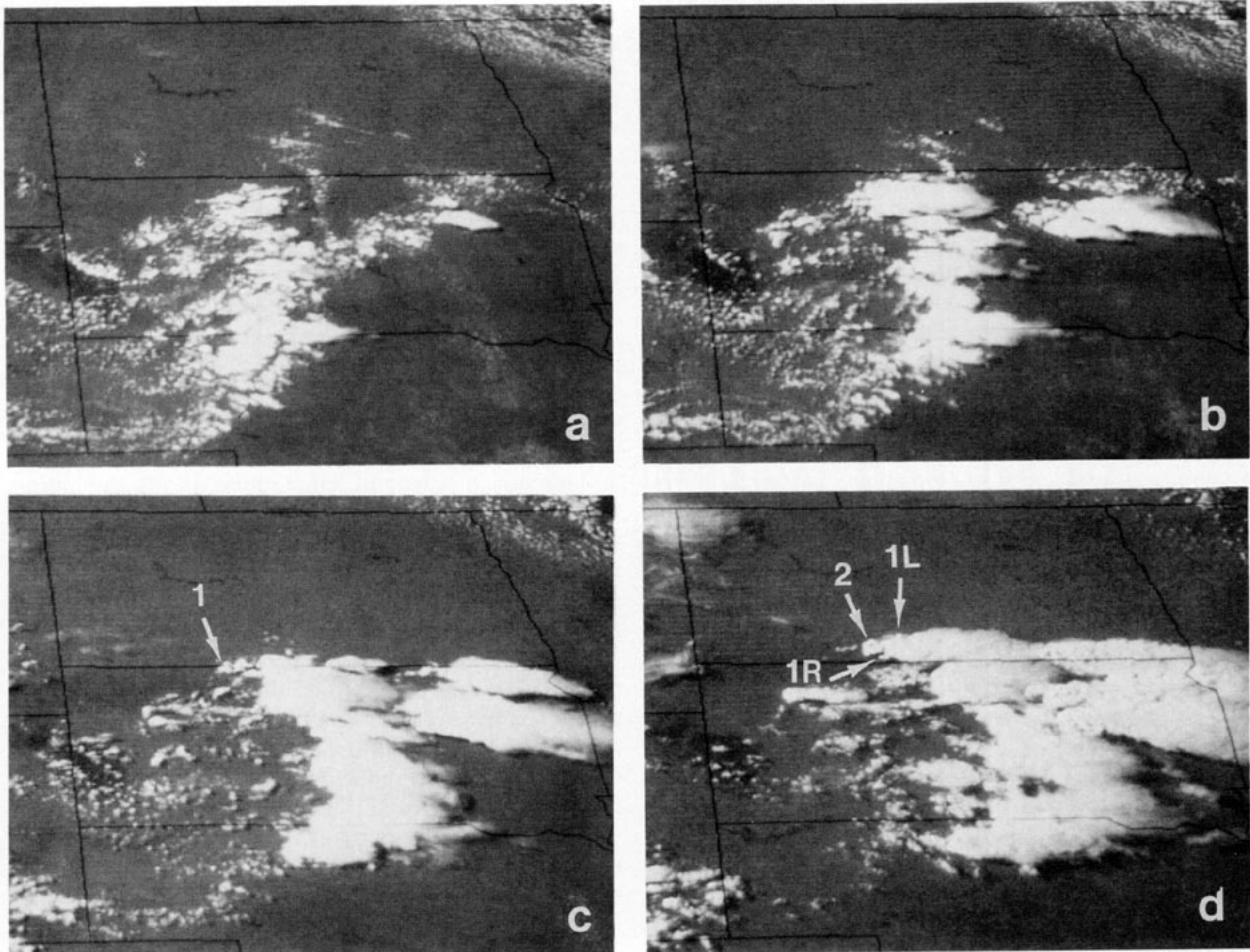


FIG. 3. Visual GOES-7 satellite photographs of cloud evolution over the Dakotas area at (a) 1501, (b) 1601, (c) 1716, and (d) 1831 CST 27 June 1989. Standing Rock storms 1 and 2 are identified with arrows; L and R indicate the left- and right-moving members of storm 1.

Klemp 1982). There is some curvature to the hodograph in the lowest 3 km that suggests that the right-moving member of a splitting storm pair should be more dominant than the left-moving member. According to Brown (1993), the nearly uniform wind layer from 3 to 8 km is the type found within, but not necessarily limited to, supercell thunderstorm environments.

Davies-Jones et al. (1990) proposed two empirical criteria for mesocyclone (rotating updraft) formation, namely, that the storm-relative winds in the lowest 3 km should be at least  $10 \text{ m s}^{-1}$  and that they should veer by at least  $90^\circ$  through the same depth. Winds relative to Standing Rock storms 1R and 2R in Fig. 6 satisfy only one or the other of these criteria. Likewise, winds relative to left-moving storms 1L and 2L satisfy only the  $90^\circ$  change of direction criterion for mesocyclone formation (where veering winds are replaced by backing winds). Therefore, theory indicates that the

updrafts in storms 1 and 2 may not develop significant rotation.

Since the composite hodograph in Fig. 6 represents conditions north of the Standing Rock storms and the other preexisting thunderstorms, it properly can be used only to deduce flow toward the left flanks of storms 1L and 2L. Air approaching the right flanks of storms 1R and 2R likely was modified by the low-altitude outflow from the nearby storms to the southeast and east.

## 5. Storm evolution

Standing Rock storms 1 and 2 were the storms within which dual-Doppler data were collected using the airborne and ground-based radars. Of the eight dual-Doppler analysis times, the wind and reflectivity fields at 7-km height for six nearly equally spaced times are shown in Fig. 7. At the earliest analysis time (1822), storm 1 shows an elongation of the 20-

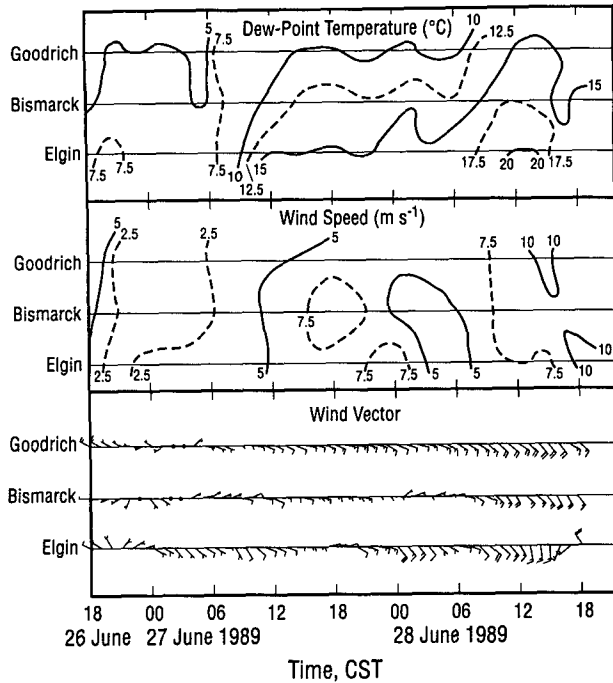


FIG. 4. Space-time cross sections of dewpoint temperature ( $^{\circ}\text{C}$ ), wind speed ( $\text{m s}^{-1}$ ), and wind vectors (long barb is  $5 \text{ m s}^{-1}$ ) from 1800 CST 26 June through 1800 CST 28 June 1989. As can be seen in Fig. 1, the cross section extends in a southwest to northeast direction from Elgin through Bismarck to Goodrich.

dBZ contour normal to the mean wind direction, as is typical of storms that are starting to split (e.g., Achtemeier 1969). The dual-Doppler coverage area did not reach the main portion of storm 1, because the aircraft turned toward the perpendicular to the viewing direction of the CP-3 radar. Though the western portion of storm 2 has missing winds owing to the proximity to the aircraft track, the winds in the rest of the storm seem to indicate that the midaltitude flow was around the storm's core. Stronger winds are indicated along the north and south edges of the storm, and weaker winds are evident in the wake region downstream of the storm's center.

By 1833 CST, the midaltitude reflectivity field associated with storm 1 had split into two identifiable entities (labeled 1L for the left member and 1R for the right member). Air downstream of the left member shows confluence into the wake region. With time, storms 1L and 1R moved farther apart and, unlike the typical splitting storm, storm 1L was the larger and longer-lasting member of the pair.

Though not complete, dual-Doppler coverage of storm 2 was more consistent. As the storm started to split at 1844 CST, enhanced midaltitude flow was maintained on the left side of the left member and on the right side of the right member. The wind speed

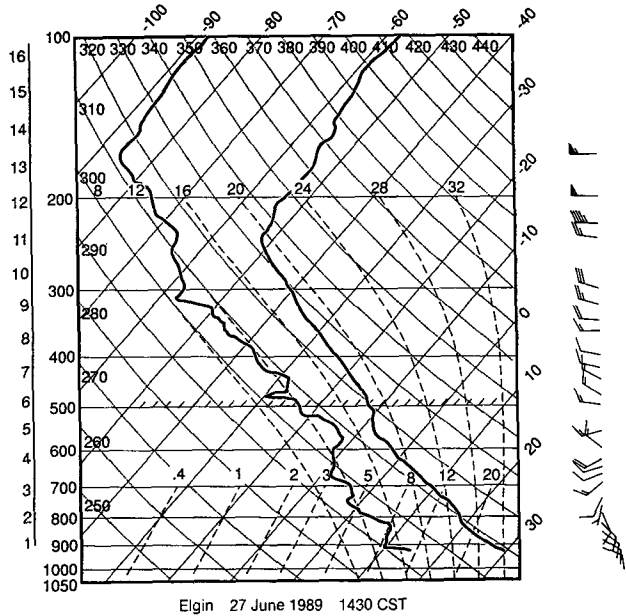


FIG. 5. Temperature, dewpoint temperature, and winds from the sounding released at Elgin at 1430 CST 27 June 1989. The long wind barb is  $5 \text{ m s}^{-1}$  and the flag is  $25 \text{ m s}^{-1}$ . Heights are in kilometers above sea level.

minimum between the two members was maintained during the splitting process through 1854 and was still somewhat apparent at 1905 CST. Throughout the splitting process, the cross-stream variation of the horizontal wind (that is, wind speed minimum in the middle and maxima on the left and right sides) suggested the presence of cyclonic vertical vorticity (where wind speed decreases from right to left) associated with the

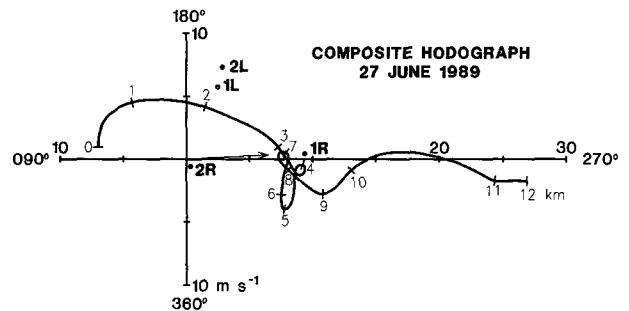


FIG. 6. Composite hodograph computed from the 1430 CST Elgin and 1800 CST Bismarck rawinsonde releases on 27 June 1989. Arrow is the mean wind vector in the 1–12-km layer. Dots indicate the tips of the storm motion vectors for the left (L) and right (R) portions of storms 1 and 2 plotted relative to the hodograph origin; storm motion was determined from the locations of the peak heights of sequential updrafts within each storm.

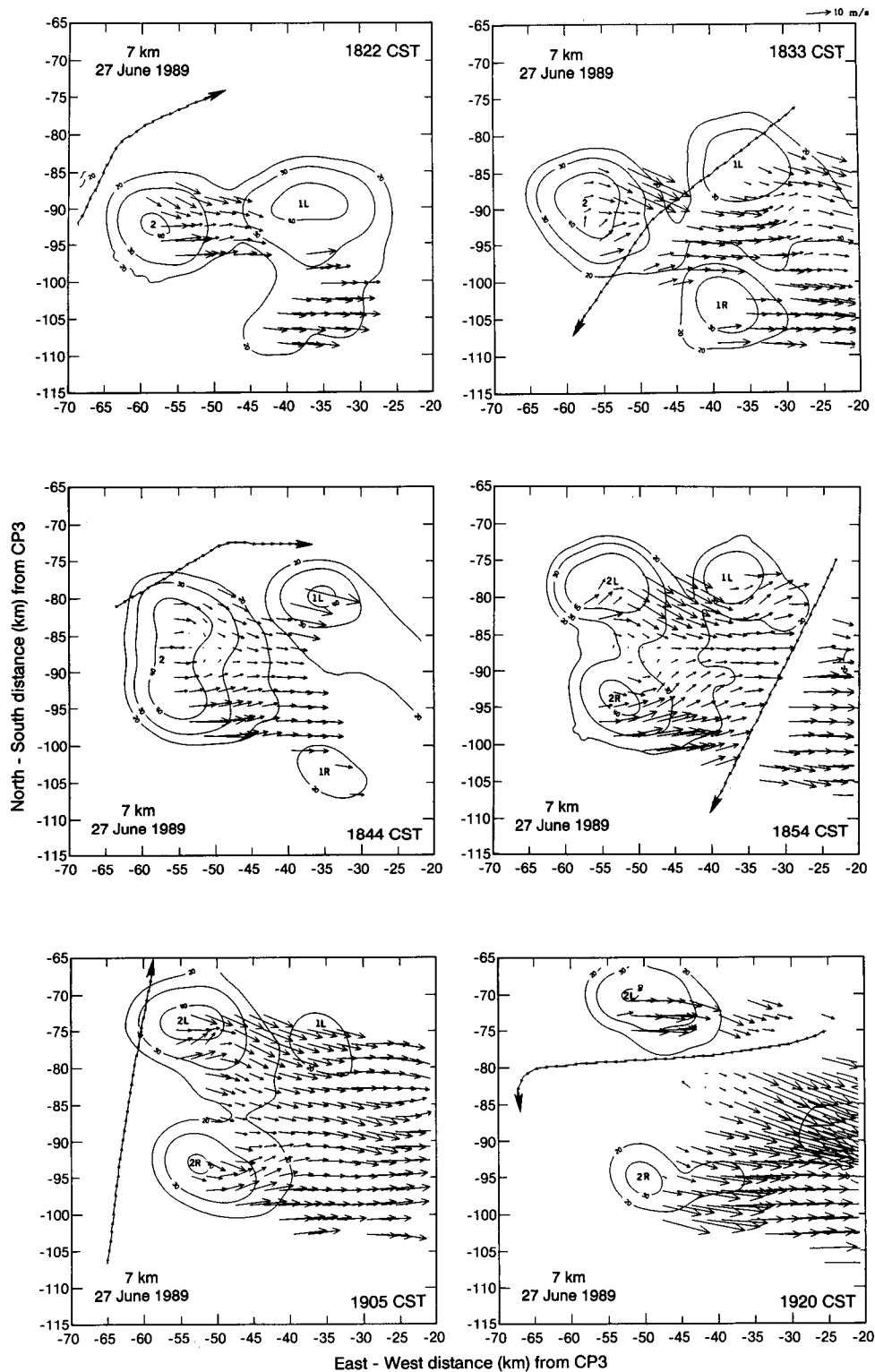


FIG. 7. Radar reflectivity contours (20, 30, and 40 dBZ) and radar-relative horizontal wind vectors (synthesized from dual-Doppler radar measurements) at a height of 7 km above the ground at reference times (a) 1822, (b) 1833, (c) 1844, (d) 1854, (e) 1905, and (f) 1920 CST 27 June 1989. Length of vector at upper-right corner represents  $10 \text{ m s}^{-1}$ . The portion of the WP-3D flight track used in the dual-Doppler analysis is indicated.

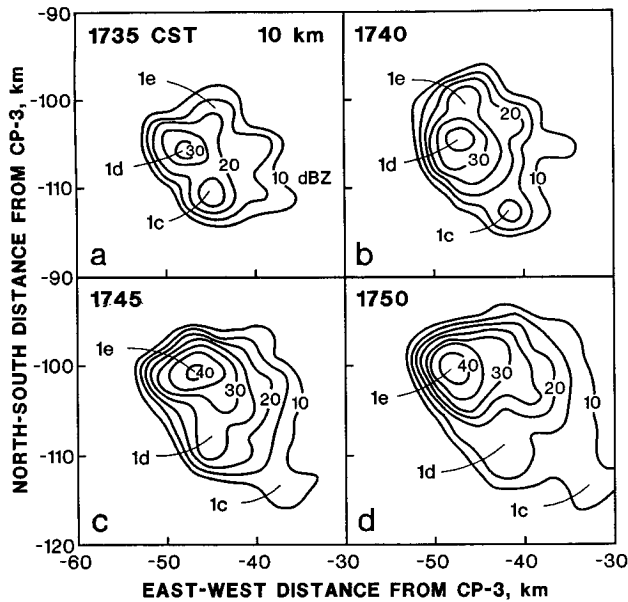


FIG. 8. Example of evolution of radar reflectivity features at 10-km height associated with the evolution of deduced updrafts 1c–1e.

right member and anticyclonic vorticity (where wind speed decreases from left to right) associated with the left member. Based on the limited number of single- and dual-Doppler radar studies of splitting storms, these deduced vorticity fields are consistent with the observations of cyclonically rotating updrafts in right-moving storms and anticyclonically rotating updrafts in left-moving storms. However, detailed single-Doppler radar observations discussed in the next section do not give any indication of updraft rotation in either splitting storm.

### 6. Deduced updraft evolution

#### a. Single-Doppler radar signatures of updrafts

Updraft positions had to be estimated using the locations of peak reflectivity values and single-Doppler velocity divergence signatures near updraft summits, because (a) neither updraft magnitude nor evolution within storms 1 and 2 was available from the airborne WP-3D and ground-based CP-3 Doppler radars owing to inadequate dual-Doppler coverage, and (b) the storms were too distant from the CP-4 Doppler radar to provide acceptable spatial resolution for dual-Doppler coverage by CP-3 and CP-4. Kingsmill and Wakimoto (1991) showed, in their multiple-Doppler radar study of a severe thunderstorm developing within a weakly sheared environment, that updraft and reflectivity summits typically were within a kilometer of each other and were associated with the rising turret of the

visible cloud. In this study, the single-Doppler radar data collected by the ground-based CP-3 radar at 3–5-min intervals provided sufficient temporal and spatial resolution to deduce the evolution and relative strengths of the updrafts. With rising reflectivity maxima being used to indicate the locations of updraft summits, the following terms are used interchangeably: reflectivity maximum, reflectivity signature of updraft, deduced updraft, and updraft.

The typical evolution of successive updrafts as indicated by radar reflectivity patterns is illustrated in Fig. 8 for storm 1. Although it might appear that there was a single updraft with small-scale perturbations, close examination of the reflectivity data in four dimensions reveals a series of updrafts that form successively on the storm's left flank. At 1735 CST, reflectivity maximum 1c was just starting to descend after reaching its maximum height. At successive 5-min intervals, it changed from a reflectivity peak to a right-flank protrusion as it moved downstream (toward the east-southeast) and continued to descend. Maximum 1d reached its greatest height at 1740 CST and likewise changed into a protrusion as it descended and moved downstream. Reflectivity maximum 1e made its initial appearance as a left-flank protrusion and continued to grow in intensity and height until reaching maximum vertical extent just after 1750 CST. It was common, especially in storm 1, for the reflectivity signature to move very slowly as it was growing vertically, but after it started to descend it would increase speed and move downstream basically with the ambient flow.

Since the divergence signature near storm top provides a direct indication of updraft location, it was used to verify the reflectivity estimate of the center of the updraft whenever it was present. At the height where the divergence signature was most pronounced (typically a few kilometers below storm top), a comparison was made between the center of the signature and the corresponding center of the reflectivity maximum for each updraft at each reference time in both storms 1 and 2. The distribution of reflectivity signature centers relative to the corresponding divergence signature centers is shown in Fig. 9. Of the 76 comparisons, 21 of the reflectivity maxima were collocated with the center of the divergence signature. A total of 66 reflectivity maxima were within 2 km of the corresponding divergence center and the remaining 10 were located 2–4 km to the east through south. If precipitation particles (represented by a reflectivity maximum) were carried a few kilometers downwind relative to the updraft, the hodograph in Fig. 6 indicates that they would move slightly south of east.

Interpretation of the horizontal flow fields within the storms is based on single-Doppler velocity measurements. Since each single-Doppler velocity data point is a one-dimensional (that is, radial component) representation of the three-dimensional flow field at that lo-

cation in space, there is no unique way to reconstruct the three-dimensional velocity vector at that location. However, when presented in a quasi-horizontal two-dimensional display, there are a number of assumptions that can be made to reconstruct a plausible two-dimensional flow field (e.g., Lemon et al. 1978). Also, there are single-Doppler velocity signatures that can be interpreted to represent specific horizontal flow patterns (e.g., Donaldson 1970; Brown and Wood 1983, 1991). Some of these signatures within a thunderstorm represent axisymmetric convergence at the bottom of an updraft (top of a downdraft), axisymmetric divergence at the top of an updraft (bottom of a downdraft), axisymmetric rotation within an updraft or downdraft, and a pair of counterrotating axisymmetric vortices (rotating about vertical axes) on the midaltitude flanks of a strong updraft. These types of signatures form the basis for issuing severe thunderstorm warnings based on single-Doppler velocity observations.

An example of the vertical distribution of single-Doppler velocity signatures associated with a nonrotating updraft is shown in Fig. 10 for updraft 1g in storm 1 at 1818 CST. The figure shows single-Doppler velocity signatures of convergence, a vortex pair, and divergence at 1, 7, and 12 km, respectively. Superimposed on each signature is a hypothetical flow field that could result when a representative Doppler velocity value (for example, 3, 5, and  $8 \text{ m s}^{-1}$ , respectively) was added to the signature at each height to make the signature more balanced with zero Doppler velocity at the center; this process produces a feature-relative flow field at each height. The convergence signature at 1 km shows a maximum of flow away from the radar ( $+1 \text{ m s}^{-1}$ ) on the near side (north side) of the signature and a maximum of flow toward the radar ( $-7 \text{ m s}^{-1}$ ) on the far side (south side). At 12-km height, the opposite is true. The divergence signature shows a maximum of flow toward the radar ( $-15 \text{ m s}^{-1}$ ) on the near side and a minimum of flow toward the radar ( $-1 \text{ m s}^{-1}$ ) on the far side. Note that the center of the 25-dBZ contour at 12 km was about 1 km to the east-southeast of the center of the divergence signature.

The single-Doppler velocity signature at 7 km for the vortex pair is more complicated. When the radar is viewing the updraft essentially perpendicular to the environmental flow direction, as in this case, the signature ideally is like a four-leaf clover of alternating sign [compare with the idealized  $280^\circ$  panels in Figs. 18 and 19 of Brown and Wood (1991)]. On the near side (north side) of the updraft, flow is toward the radar (negative extreme), and then away from the radar (positive extreme) as the ambient air flows around the updraft. If the updraft were centered on this negative-positive couplet, the signature would be called a "mesoanticyclone signature." On the far side (south side), flow is away from the radar (positive extreme), and then toward the radar (negative extreme). If the updraft

were centered on this positive-negative couplet, the signature would be called a "mesocyclone signature." Since the centers of the upper-altitude divergence and reflectivity signatures are nearly vertically aligned with the center of the col between the two pairs of positive and negative extremes, one deduces that the midaltitude updraft was located between the two vorticity centers and therefore had insignificant net rotation. If the reflectivity signature had been in error by an extreme of 2–4 km, the error would have been in a southeasterly direction (Fig. 9), which is normal to the direction needed to move the updraft from the center of the col to the center of cyclonic or anticyclonic rotation. The relative relationships shown in Fig. 9 are similar for all updrafts in these storms. Therefore, use of the center of the upper-altitude reflectivity maximum as an indicator of updraft location (center of divergence signature) should not lead to problems in discriminating between rotating and nonrotating updrafts.

#### b. Deduced updraft features in storms 1 and 2

During the growing stage of an updraft, the hydrometeors that form in its upper portions produce a localized maximum of radar reflectivity in plan view. The 15-dBZ top of this feature was used here to approximate the summit of each updraft within storms 1 and 2. As long as the 15-dBZ top was rising with time (corresponding to visual cloud turrets), one can deduce that the updraft was intensifying and increasing in altitude. When the 15-dBZ top reached its maximum vertical

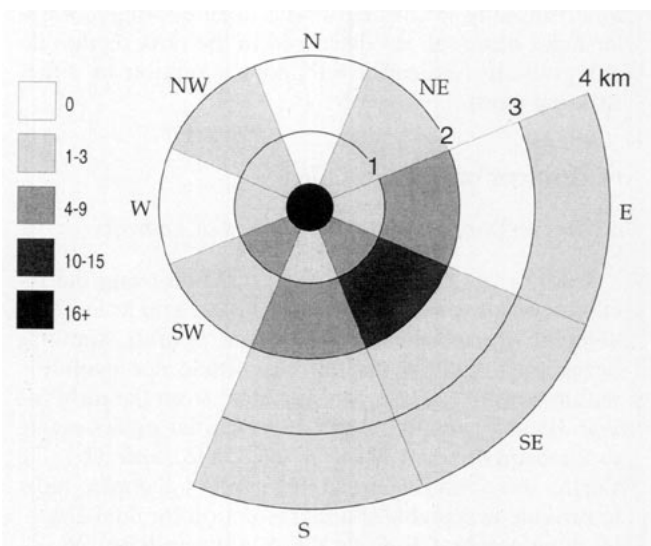


FIG. 9. Distribution of the location of the reflectivity signature of an updraft center near storm top relative to the center of the single-Doppler velocity signature of the associated divergence center. Of the 76 distinctive reflectivity-divergence pairs in storms 1 and 2, 66 were within 2 km of each other, including 21 that were coincident (black circle at the center of the distribution).

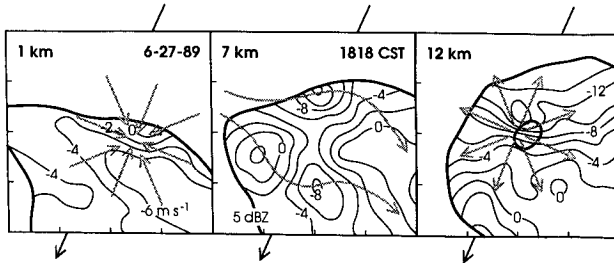


FIG. 10. Single-Doppler velocity measurements (radar-relative) at 1-, 7-, and 12-km heights within storm 1L in the vicinity of updraft 1g at 1818 CST. Superimposed streamlines represent idealized feature-relative flow. The thick outer boundaries are 5-dBZ reflectivity contours, and the small thick inner closed curve at 12 km is a 25-dBZ contour. Border tick marks are at 5-km intervals. Arrows outside each panel indicate the CP-3 Doppler radar viewing direction passing through the center of each panel.

extent and started to descend, one then can deduce that the updraft had started to die and that the radar-detectable particles probably still represent the summit of the weakening updraft. However, after a short time, the descending top no longer can be interpreted as representing an updraft, but instead should be interpreted as representing the upper portion of the descending precipitation column within the storm cloud. The reflectivity maximum associated with hydrometeors that have been descending downstream of the updraft for 10 or more minutes typically has spatial continuity down to the ground.

A time history of the tops of the primary 15-dBZ reflectivity features in Standing Rock storm 1 is shown in Fig. 11; to be called a primary feature, it generally was the tallest feature in the storm sometime during its existence. The plot in Fig. 11 indicates that successive deduced updraft summits grew to increasing heights until updraft 1e, which had the tallest and longest-lasting reflectivity feature. Subsequent updrafts grew to lesser and lesser heights until the storm dissipated with the demise of updraft 1j. Updrafts 1c–1h penetrated the tropopause by 1–4 km. The reflectivity signature of the first updraft on the storm’s right flank (1Ra) appeared 20–25 min after 1e reached its maximum vertical extent. The strongest right-flank updraft was the second of the four to occur, but none of them were strong enough to penetrate the tropopause.

None of the updrafts in the left or right portions of storm 1 ever exhibited any significant rotation. Significant rotation (mesocyclone) is defined as the collocation of an updraft with a region of Doppler velocity azimuthal shear exceeding  $5 \times 10^{-3} \text{ s}^{-1}$  or vorticity exceeding  $1 \times 10^{-2} \text{ s}^{-1}$ ; for an axisymmetric vortex with a Rankine velocity profile, vorticity is equal to twice the azimuthal shear of Doppler velocity across the single-Doppler velocity vortex signature (e.g., Brown and Wood 1991). However, nearly all the taller

(and, presumably, stronger) deduced updrafts were located within a vortex-pair signature at midaltitudes. Some of the new updrafts formed within one of the members of the vortex pair and briefly were coincident with weak azimuthal shear, but when they became strong they had their own vortex-pair signature. As the reflectivity signatures were descending, a few of them were collocated with weak azimuthal shear of one sign or the other.

The hatched portions of the curves in Fig. 11 represent the times when a midaltitude vortex-pair signature (indicative of flow around a strong updraft) coincided with an updraft signature. Of those updrafts that had 15-dBZ tops that penetrated the tropopause, only 1b and 1h did not have an associated vortex-pair signature; these generally were the more short-lived reflectivity features. Of the updraft signatures that did not reach the tropopause, only 1Rb had an associated vortex-pair signature.

The horizontal projections of the 15-dBZ tops in Fig. 11 are plotted in Fig. 12. These features (representing updrafts and then downdrafts) moved predominantly from west to east with the mean wind. The letter on each line indicates the location of maximum vertical extent for that updraft signature. It is apparent from Figs. 11 and 12 that each 15-dBZ top remained essentially stationary during its growth phase and then moved downwind following updraft demise as the reflectivity maximum descended in conjunction with the descent of precipitation particles.

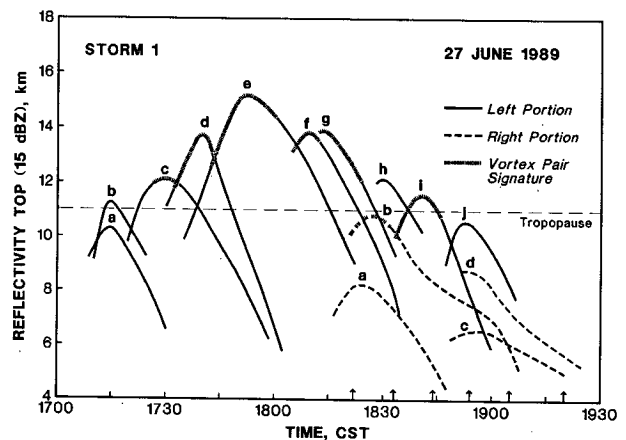


FIG. 11. Time–height plots of the 15-dBZ tops of radar reflectivity features associated with deduced updrafts in storm 1. Solid curves represent features in the initial left member and dashed curves represent features in the right member. Hatched portions of the curves indicate the times when there were single-Doppler velocity signatures of vortex pairs at midaltitudes (indicating horizontal flow around both sides of the updraft). Vertical arrows along the abscissa indicate the times of the dual-Doppler data presented in Fig. 7. Tropopause height (dashed) is a representative height derived from the various soundings made on 27 June.

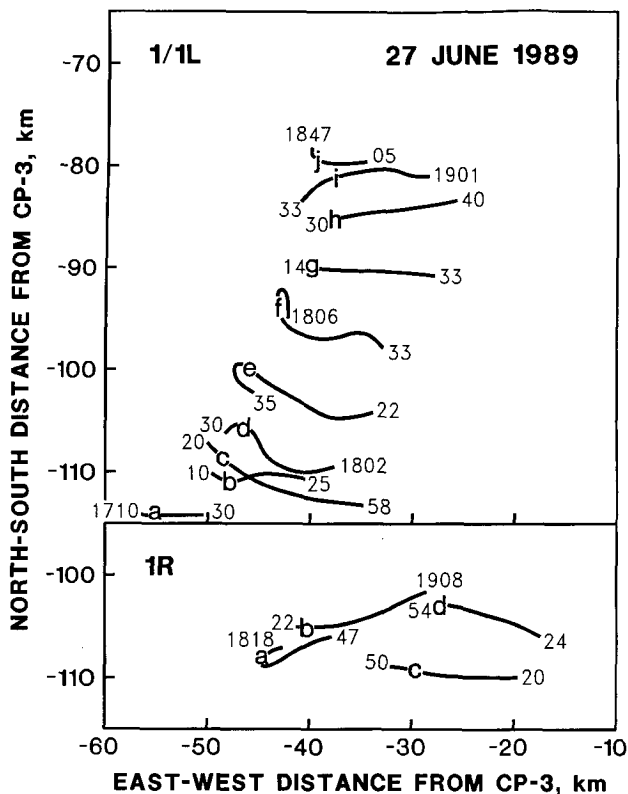


FIG. 12. Horizontal projections of the reflectivity signatures of updrafts shown in Fig. 11, with beginning and ending times indicated. The letter identifying each deduced updraft is placed at that point along the curve where the reflectivity signature had its maximum vertical extent.

The horizontal projections in Fig. 12 indicate that storm 1/1L propagated to the left from the very beginning, because new updrafts consistently formed on the left flank. Storm 1R propagated more in the downwind direction rather than exhibiting pronounced propagation to the right of the mean wind.

Vertical and horizontal evolution of the 15-dBZ tops of the reflectivity features in storm 2 is shown in Figs. 13 and 14. The overall evolution was the same as for storm 1. The tallest reflectivity feature was associated with updraft 2c. About 10 min after updraft 2c reached its maximum vertical extent, a new updraft formed on the storm's right flank. In all, three significant updrafts appeared in storm 2R, and the first one was the strongest. Each of them formed at essentially the same ground-relative location. All updraft signatures within storms 2/2L and 2R exceeded 10 km in height, and all of them, except for updraft 2b, coincided with a midaltitude vortex-pair signature. None of the updrafts in these storms exhibited any significant rotation.

The evolution of storms 1 and 2 on the radar display (not shown) suggests that both storms formed along an outflow boundary that spread out from thunderstorms

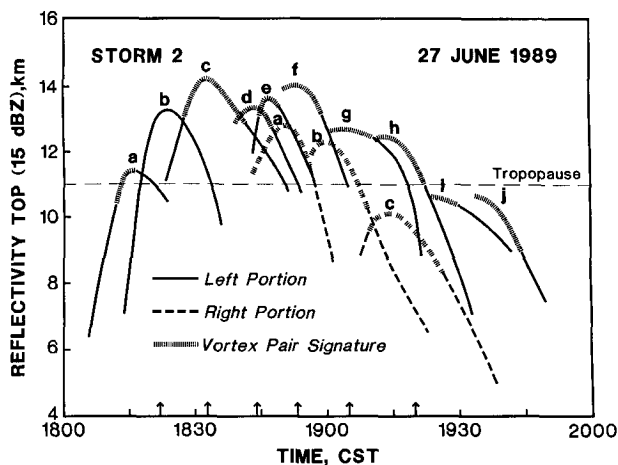


FIG. 13. Same as Fig. 11 except for storm 2.

a few tens of kilometers to their east and southeast (see Fig. 3). However, the outflow boundaries from storms 1 and 2 that triggered the series of new left-flank and right-flank updrafts were not detectable in the radar data. By comparing the initial location of new updrafts with the edge of the storm, one can surmise the location of the triggering gust front. The initial location aloft of the reflectivity signature for each new updraft relative

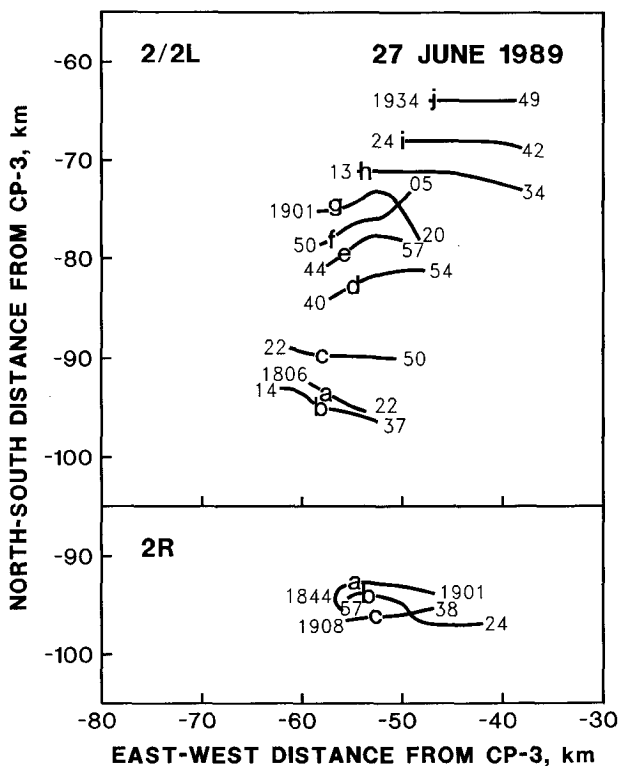


FIG. 14. Same as Fig. 12 except for storm 2.

to the 20-dBZ radar reflectivity contour at 1-km height (approximating the edge of the storm) in storms 1/1L and 2/2L is shown in the top parts of Figs. 15 and 16. The figures indicate that each new updraft signature in the initial and subsequent left portions of the storms formed above or within a few kilometers of the left edge of the storms. Similarly, the updraft signatures within storms 1R and 2R formed within a few kilometers of the right edge of the storms (bottom part of Figs. 15 and 16). These data suggest that the formation of the right member of each splitting storm was delayed until after the subcloud cold pool had built up enough for the gust front to reach the right side of the storm.

**7. Concluding discussion**

During the late afternoon and early evening of 27 June 1989, thunderstorms formed over Standing Rock Indian Reservation in the southern portion of the North Dakota Thunderstorm Project area. Two of at least three splitting storms on that day were investigated using the NOAA WP-3D airborne Doppler radar and the NCAR CP-3 ground-based Doppler radar. The result-

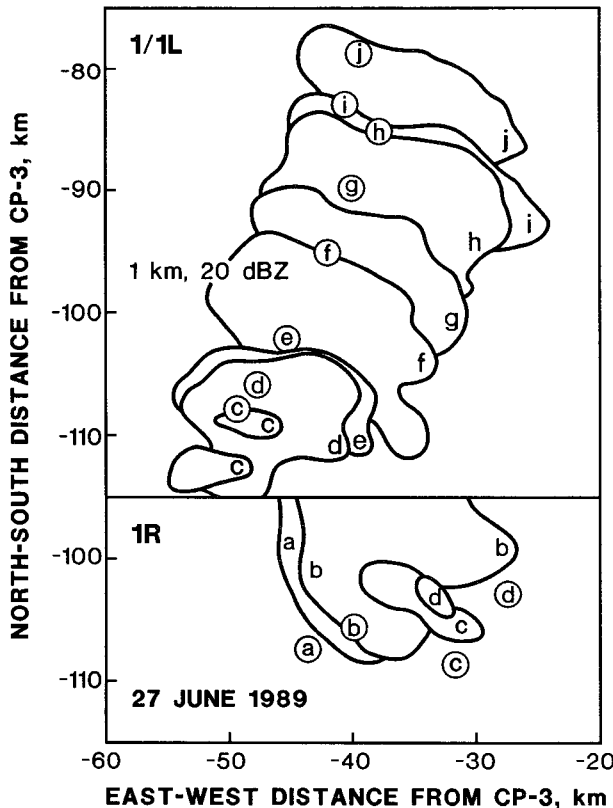


FIG. 15. Plan view of the initial location of each deduced updraft in the upper portions of storm 1 (circled letter) and the coincident 20-dBZ reflectivity contour at 1-km height (labeled with the updraft letter).

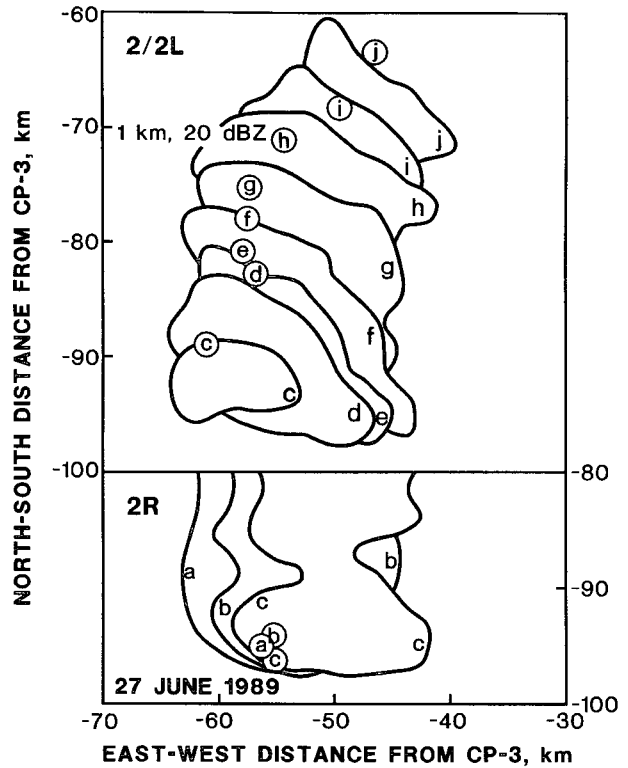


FIG. 16. Same as Fig. 15 except for storm 2.

ing dual-Doppler coverage of the actively growing portions of the storms was limited owing to the aircraft's low altitude and proximity to the storms.

Both storms 1 and 2 exhibited the same characteristics during the splitting process. Each started as a single radar echo with midaltitude air flowing around it; increased wind speed was found on the lateral flanks and decreased speed was found on the downwind side. With time, the radar reflectivity pattern elongated along an axis normal to the predominant midaltitude wind direction. As the elongation process continued, the reflectivity pattern separated into two distinct echoes that continued to move apart relative to one another. The left members moved at  $7-8 \text{ m s}^{-1}$  at an angle of about  $65^\circ$  to the left of the mean wind, while the right members moved generally with the mean wind but in a more variable manner. Deduced updrafts within both members of the two splitting storms moved essentially in the direction of the mean wind. Contrary to the usual splitting storm evolution, the left member was the dominant and longer-lasting one.

Since the updraft regions of the storms were not consistently sampled with the dual-Doppler radar system, radar measurements from the ground-based CP-3 radar were used instead to deduce updraft evolution. Peak reflectivity values near storm top were used to deduce the locations of the primary updrafts; a primary updraft

generally was defined as one that was the tallest of all reflectivity features sometime during its existence. When present, single-Doppler velocity divergence signatures near storm top were used to confirm the updraft locations. From the very beginning of both initial storms, each new updraft formed on the left flank of an existing updraft. The average interval between successive updrafts was 11 min (with a range of 3–31 min). The updrafts grew to increasingly greater heights until one reached maximum vertical extent 30%–40% of the way through the storm's life cycle. Successive updrafts then grew to lesser and lesser heights until the precipitation from the last left-flank updraft fell out about 2 h after the storm first appeared on radar.

The first right-flank updraft appeared on radar 10–20 min after the tallest left-flank updraft signature started to descend. The average interval between successive right-flank updrafts was 12 min (with a range of 4–28 min). The right-flank storms lasted only about 1 h, and their tallest tops were considerably shorter than those for the left-flank storms.

Neither member of either splitting storm had any rotating updrafts, contrary to what typically has been found from Doppler velocity measurements in a limited number of splitting storms. Of the left- and right-flank updrafts in storms 1 and 2 that extended upward beyond 10 km, 80% produced single-Doppler velocity signatures of a vortex pair, with the vertical vorticity centers on the left and right sides of the updrafts. The signatures typically were limited to the height interval from 6 to 8 km and never extended below 5 km or above 9 km. Vorticity values associated with the vortex-pair signatures typically were  $\pm 2 \times 10^{-3}$ – $4 \times 10^{-3} \text{ s}^{-1}$ , with a rare extreme value of  $\pm 5 \times 10^{-3}$ – $6 \times 10^{-3} \text{ s}^{-1}$ .

It is interesting to hypothesize about what controlled the propagational characteristics and relative timing of the left- and right-flank updrafts in the Standing Rock storms. Low-altitude convergence along cold-air outflow boundaries plays an important role in the initiation and maintenance of updrafts within convective storms (e.g., Thorpe and Miller 1978; Weaver 1979; Wilhelmson and Chen 1982). Since the initial updrafts within Standing Rock storms 1 and 2 formed on the left side, it is likely that the cold surface outflow air initially was able to extend only beyond the left edge of the storm and interact with gust-front-relative flow approaching the storm at low altitudes. There also may have been a contribution from cold-air outflow from the storms immediately to the east and southeast. Subsequent sequential updrafts led to the formation of precipitation downdrafts that systematically reinvigorated the surface cold pool. It is likely that the increasing mass of surface cold air associated with those downdrafts permitted the gust front to eventually extend to the right edge of the storm. Outflow air from the storms to the east and southeast also may have retarded the low-al-

titude outflow toward the right flank. Gust-front-relative flow approaching the right side of the storm likely produced a region of low-altitude convergence that led to the formation of the initial right-flank updraft. The right member of the split then developed its own precipitation-cooled and evaporatively cooled air, and gust front, and was able to maintain its own regeneration mechanism as the left member moved away.

The above discussion also provides some clues to why the left-moving storms were the dominant members of the splitting storms on 27 June 1989. Based on the hodograph in Fig. 6, which to a first approximation is a straight hodograph, one would expect a balanced pair of splitting storms to be produced (e.g., Rotunno and Klemp 1982). To a higher approximation, hodograph curvature in the lowest 3 km indicates that there was greater storm-relative/gust-front-relative environmental flow toward the right flank of the right members than toward the left flank of the left members, even though both storm-relative/gust-front-relative flows are relatively weak. If, indeed, cooler, more stable outflow from the nearby storms retarded low-altitude rightward-moving outflow from storms 1 and 2, then it also could have decreased the amount of buoyant energy available for right-flank updrafts, resulting in shallower and shorter-lived right-flank storms. A dual-Doppler radar study of Standing Rock storm 3, which is under way, may provide some answers to the questions concerning the dominance of the left-moving storms on 27 June 1989.

*Acknowledgments.* Special thanks go to Dr. Bradley Smull of the National Severe Storms Laboratory (NSSL, Boulder) for the enormous amount of time he spent both in training the authors on the use of the airborne Doppler radar editing programs and in consulting on problems that occurred while testing some of the programs. Thanks also to Dr. David Jorgensen (NSSL, Boulder) for his help in interpreting the airborne data. Robert Hueftle (NSSL, Boulder) was helpful in making many changes to existing programs and was always available when problems occurred. Melissa Hornecker and Kathleen Eyeran (NSSL, Norman, Oklahoma) assisted with the editing and processing of the CP-3 Doppler radar data for the single-Doppler radar portion of this study. We appreciate the detailed reviews of the manuscript by Drs. Erik Rasmussen (NSSL, Norman), Thomas Christian (Wave Propagation Laboratory), and an anonymous reviewer. The North Dakota Thunderstorm Project was sponsored by the NOAA Federal-State Cooperative Program in Atmospheric Modification Research, the North Dakota Atmospheric Resource Board (NDARB), and the National Science Foundation. We especially appreciate the support and encouragement of Project Director Bruce Boe of the NDARB.

TABLE A1. Characteristics of post-split severe thunderstorms. Associated severe weather: H—hail, W—damaging wind, and T—tornado.

Date	Location	Storm	Approximate lifetime (h)	Severe weather	Maximum deviation (deg) from mean wind	Average speed (m s <sup>-1</sup> )	Mean wind computation technique	Source
27 July 1956	Quebec	Ia	2	—	8 L	15	700 mb (3 km)	Hitschfeld (1960)
		Ib	2	—	43 R	13		
		Ia'	1	—	29 L	17		
		Ia''	1	—	8 R	14		
24 May 1962	Oklahoma	a	3		21 L	18	900–200 mb (1–12 km) pressure weight	Newton and Fankhauser (1964)
		B	8	H, W, T	53 R	9		
3 April 1964	Texas–Oklahoma	A <sub>1</sub>	2		34 L	13	sfc–300 mb (0–9 km) pressure weight	Wilk (1966); Fujita and Grandoso (1968); Charba and Sasaki (1971)
		A <sub>2</sub>	1		21 R	11		
		A <sub>2</sub>	2		10 L	16		
		C <sub>2</sub>	2	H, W, T	15 R	11		
		A <sub>3</sub>	3	H	44 L	17		
		C <sub>3</sub>	3	H, T	19 R	13		
		A <sub>4</sub>	1		13 L	21		
23 April 1964	Oklahoma	D	1	H, W, T	20 L	16	850–300 mb (1.5–9 km) pressure weight	Hammond (1967)
		F	1		0 R	14		
27 May 1965	Oklahoma	L	2	H, T	35 L	15	storm depth	Harrold (1966)
		R	3	H, T	35 R	10		
25 August 1965	Iowa–Illinois	C3	3	H, W	32 R	10		Achtemeier (1969)
		C8	—	H	25 R	13		
		C9, 11	3	H	17 L	18		
		C17	1	H	21 R	15		
		C18	1	H	15 L	23		
		E1	3	H, W, T	15 R	8		
		E2	2	H	48 L	17		
		E4	—	H, T	12 R	13		
		E5	—	H	40 L	20		
26 August 1965	Iowa	S2	2	H	29 L	26		Achtemeier (1969)
		S1	>3	H, T	16 R	19		
16 April 1967	Oklahoma	A	2	H	15 L	17	950–200 mb (0.5–12 km) pressure weight	Haglund (1969)
		D	3	H, T	35 R	14		
		L	1		—	—		
		K	3		40 R	13		
18 June 1970	Colorado	1	1		0 L	17	0–10 km	Marwitz (1972)
		2	2	H	70 R	9		
19 April 1972	Oklahoma	L	3	H	22 L	28	storm depth pressure weight	Brown et al. (1973)
		R	3	H, T	25 R	13		
27 June 1972	Oklahoma	L1	2	H, W, T	47 L	16		Achtemeier [1976, personal communication; from Burgess et al. (1976)]
		R1	2		25 R	10		
		L2	2	H	35 L	16		
		R2	2		22 R	11		
24 May 1973	Oklahoma	L	2	H	28 L	15	1–12 km pressure weight	Burgess et al. (1976); Lemon et al. (1978)
		R	2	H, T	12 R	10		
30 May 1976	Oklahoma	L	1	H	54 L	14	density weight	Lemon and Burgess (1980); Burgess (1981)
		R	3	H, T	222 R*	4		
1 May 1977	Oklahoma	L	1		60 L	6	1–12 km density weight	Bluestein and Sohl (1979)
		R	1	H	54 R	3		
29 April 1978	Oklahoma	DLM	1	—	18 L	19	1–11 km density weight	Adams (1981, personal communication)
		DRM	1	—	76 R	4		
		KLM	1	—	38 L	18		
		KRM	1	—	56 R	5		
6 June 1979	Oklahoma	L	3		20 L	16	1–11 km density weight	Brown (1992)
		R	3	H	7 R	11		
1 August 1981	Montana	L	>2		32 L	21	3–12 km	Kubesh et al. (1988)
		R	>5	H	7 R	9		
26 April 1984	Oklahoma	L	2		22 L	24	1–10 km density weight	Burgess and Curran (1985)
		R	4	H, W, T	1 R	17		
13 June 1984	Colorado	A1	>1		13 L	9	0–6 km density weight	Conway and Weisman (1988)
		A	3	H	53 R	5		
		E1	<1		2 L	10		
		E	<1		47 R	2		

\* Storm direction is so anomalous that it is not included in Table 1 computations.

## APPENDIX

## Characteristics of Splitting Thunderstorms

Burgess et al. (1976) compiled a list of 16 splitting storm pairs from the literature that itemized such storm characteristics as the lifetime, associated severe weather, directional deviation of storm motion from the mean wind, and storm speed for both members of each splitting storm pair. Their compilation has been updated to include a total of 31 splitting storm pairs that are listed in Table A1.

Included in Table A1 is a listing of the methods used to determine the mean wind, from which the deviant storm motion was computed; not all sources mentioned the computation method. In most cases, a weighted mean value was computed over most of the storm depth; the overall height interval is listed in the table. To account for the decrease of air density with height, the means either were computed from values at uniform pressure intervals (referred to as "pressure weighting" in the table) or from values at uniform height intervals that were weighted by the density at those heights (referred to as "density weighting").

The data compiled in Table A1 are summarized in Table 1.

## REFERENCES

- Achtemeier, G. L., 1969: Some observations of splitting thunderstorms over Iowa on August 25–26, 1965. Preprints, *Sixth Conf. on Severe Local Storms*, Chicago, Amer. Meteor. Soc., 89–94.
- Bluestein, H. B., and C. J. Sohl, 1979: Some observations of a splitting severe thunderstorm. *Mon. Wea. Rev.*, **107**, 861–878.
- , and G. R. Woodall, 1990: Doppler-radar analysis of a low-precipitation severe storm. *Mon. Wea. Rev.*, **118**, 1640–1664.
- Boe, B. A., and H. L. Johnson, 1990: Destabilization antecedent to a tornadic northern High Plains mesoscale convective system: A case study. Preprints, *16th Conf. on Severe Local Storms*, Kananaskis Park, Alberta, Canada, Amer. Meteor. Soc., 538–541.
- , J. L. Stith, P. L. Smith, J. H. Hirsch, J. H. Helsdon, Jr., A. G. Detwiler, H. D. Orville, B. E. Martner, R. F. Reinking, R. J. Meitin, and R. A. Brown, 1992: The North Dakota Thunderstorm Project: A cooperative study of High Plains thunderstorms. *Bull. Amer. Meteor. Soc.*, **73**, 145–160.
- Brown, R. A., 1992: Initiation and evolution of updraft rotation within an incipient supercell thunderstorm. *J. Atmos. Sci.*, **49**, 1997–2014.
- , 1993: A compositing approach for preserving significant features in atmospheric profiles. *Mon. Wea. Rev.*, **121**, 874–880.
- , and V. T. Wood, 1983: Improved severe storm warnings using Doppler radar. *Natl. Wea. Dig.*, **8**(3), 17–27; Errata, **9**(1), 2.
- , and —, 1991: On the interpretation of single-Doppler velocity patterns within severe thunderstorms. *Wea. Forecasting*, **6**, 32–48.
- , D. W. Burgess, and K. C. Crawford, 1973: Twin tornado cyclones within a severe thunderstorm: Single Doppler radar observations. *Weatherwise*, **26**, 63–69, 71.
- , C. R. Safford, S. P. Nelson, D. W. Burgess, W. C. Bumgarner, M. L. Weible, and L. C. Fortner, 1981: Multiple Doppler radar analysis of severe thunderstorms: Designing a general analysis system. NOAA Tech. Memo. ERL NSSL-92, National Severe Storms Laboratory, Norman, OK, 18 pp. [NTIS PB82-113117.]
- Burgess, D. W., 1981: Evidence for anticyclonic rotation in left-moving thunderstorms. Preprints, *20th Conf. on Radar Meteorology*, Boston, Amer. Meteor. Soc., 52–54.
- , and E. B. Curran, 1985: The relationship of storm type to environment in Oklahoma on 26 April 1984. Preprints, *14th Conf. on Severe Local Storms*, Indianapolis, IN, Amer. Meteor. Soc., 208–211.
- , L. R. Lemon, and G. L. Achtemeier, 1976: Severe storm splitting and left-moving storm structure. The Union City Tornado of 24 May 1973, NOAA Tech. Memo. ERL NSSL-80, National Severe Storms Laboratory, Norman, OK, 53–66. [NTIS PB-269443/AS.]
- Charba, J., and Y. Sasaki, 1971: Structure and movement of the severe thunderstorms of 3 April 1964 as revealed from radar and surface mesonet network data analysis. *J. Meteor. Soc. Japan*, **49**, 191–214.
- Conway, J. W., and M. L. Weisman, 1988: An investigation into the splitting and propagation of the 13 June 1984 Denver hailstorms. Preprints, *15th Conf. on Severe Local Storms*, Baltimore, MD, Amer. Meteor. Soc., 276–279.
- Davies-Jones, R. P., D. Burgess, and M. Foster, 1990: Test of helicity as a tornado forecast parameter. Preprints, *16th Conf. on Severe Local Storms*, Kananaskis Park, Alberta, Canada, Amer. Meteor. Soc., 588–592.
- Donaldson, R. J., Jr., 1970: Vortex signature recognition by Doppler radar. *J. Appl. Meteor.*, **9**, 661–670.
- Eilts, M. D., and S. D. Smith, 1990: Efficient dealiasing of Doppler velocities using local environment constraints. *J. Atmos. Oceanic Technol.*, **7**, 118–128.
- Fujita, T., and H. Grandoso, 1968: Split of a thunderstorm into anticyclonic and cyclonic storms and their motion as determined from numerical model experiments. *J. Atmos. Sci.*, **25**, 416–439.
- Haglund, G. T., 1969: A study of a severe local storm of 16 April 1967. ESSA Tech. Memo. ERLTM-NSSL 44, National Severe Storms Laboratory, Norman, OK, 54 pp. [NTIS PB-184970.]
- Hammond, G. R., 1967: Study of a left moving thunderstorm of 23 April 1964. ESSA Tech. Memo. IERTM-NSSL 31, National Severe Storms Laboratory, Norman, OK, 75 pp. [NTIS PB-174681.]
- Harrold, T. W., 1966: A note on the development and movement of storms over Oklahoma on May 27, 1965. ESSA Tech. Memo. IERTM-NSSL-29, National Severe Storms Laboratory, Norman, OK, 1–8. [NTIS AD-644899.]
- Hitschfeld, W., 1960: The motion and erosion of convective storms in severe vertical wind shear. *J. Meteor.*, **17**, 270–282.
- Jorgensen, D. P., P. H. Hildebrand, and C. L. Frush, 1983: Feasibility test of an airborne pulse-Doppler meteorological radar. *J. Climate Appl. Meteor.*, **22**, 744–757.
- Kingsmill, D. E., and R. M. Wakimoto, 1991: Kinematic, dynamic, and thermodynamic analysis of a weakly sheared severe thunderstorm over northern Alabama. *Mon. Wea. Rev.*, **119**, 262–297.
- Kubesh, R. J., D. J. Musil, R. D. Farley, and H. D. Orville, 1988: The 1 August 1981 CCOPE storm: Observations and modeling results. *J. Appl. Meteor.*, **27**, 216–243.
- Lemon, L. R., and D. W. Burgess, 1980: Magnitude and implications of high speed outflow at severe storm summits. Preprints, *19th Conf. on Radar Meteorology*, Miami Beach, FL, Amer. Meteor. Soc., 364–368.
- , —, and R. A. Brown, 1978: Tornadic storm airflow and morphology derived from single-Doppler radar measurements. *Mon. Wea. Rev.*, **106**, 48–61.
- Marwitz, J. D., 1972: The structure and motion of severe hailstorms. Part I: Supercell storms. *J. Appl. Meteor.*, **11**, 166–179.
- Newton, C. W., and J. C. Fankhauser, 1964: On the movements of convective storms, with emphasis on size discrimination in relation to water-budget requirements. *J. Appl. Meteor.*, **3**, 651–668.
- Rotunno, R., and J. B. Klemp, 1982: The influence of the shear-induced pressure gradient on thunderstorm motion. *Mon. Wea. Rev.*, **110**, 136–151.

- Thorpe, A. J., and M. J. Miller, 1978: Numerical simulations showing the role of the downdraught in cumulonimbus motion and splitting. *Quart. J. Roy. Meteor. Soc.*, **104**, 873–893.
- Vasiloff, S. V., M. H. Jain, D. L. Keller, A. Witt, V. T. Wood, P. L. Spencer, G. J. Stumpf, and M. D. Eilts, 1993: An evaluation of two Doppler radar mesocyclone detection algorithms. Preprints, *26th Int. Conf. on Radar Meteorology*, Norman, OK, Amer. Meteor. Soc., 657–659.
- Weaver, J. F., 1979: Storm motion as related to boundary-layer convergence. *Mon. Wea. Rev.*, **107**, 612–619.
- Wilhelmson, R. B., and J. B. Klemp, 1981: A three-dimensional numerical simulation of splitting severe storms on 3 April 1964. *J. Atmos. Sci.*, **38**, 1581–1600.
- , and C.-S. Chen, 1982: A simulation of the development of successive cells along a cold outflow boundary. *J. Atmos. Sci.*, **39**, 1466–1483.
- Wilk, K. E., 1966: Motion and intensity characteristics of the severe thunderstorms of April 3, 1964. ESSA Tech. Memo. IERTM-NSSL-29, National Severe Storms Laboratory, Norman, OK, 9–21. [NTIS AD-644899.]